









Pavo: Discovery of a star-forming dwarf galaxy just outside the Local Group*

MICHAEL G. JONES ¹, BURÇIN MUTLU-PAKDIL ², DAVID J. SAND ¹, RICHARD DONNERSTEIN ¹,
DENIJA CRNOJEVIĆ ³, PAUL BENNET ⁴, CATHERINE E. FIELDER ¹, ANANTHAN KARUNAKARAN ^{5,6},
KRISTINE SPEKKENS ^{7,8}, JAY STRADER ⁹, RYAN URQUHART ⁹ AND DENNIS ZARITSKY ¹

¹Steward Observatory, University of Arizona, 933 North Cherry Avenue, Rm. N204, Tucson, AZ 85721-0065, USA

²Department of Physics and Astronomy, Dartmouth College, Hanover, NH 03755, USA

³University of Tampa, 401 West Kennedy Boulevard, Tampa, FL 33606, USA

⁴Space Telescope Science Institute, 3700 San Martin Drive, Baltimore, MD 21218, USA

⁵Department of Astronomy & Astrophysics, University of Toronto, Toronto, ON M5S 3H4, Canada

⁶Dunlap Institute for Astronomy and Astrophysics, University of Toronto, Toronto ON, M5S 3H4, Canada

⁷Department of Physics and Space Science, Royal Military College of Canada P.O. Box 17000, Station Forces Kingston, ON K7K 7B4, Canada

⁸Department of Physics, Engineering Physics and Astronomy, Queen's University, Kingston, ON K7L 3N6, Canada

⁹Center for Data Intensive and Time Domain Astronomy, Department of Physics and Astronomy, Michigan State University, East Lansing, MI 48824, USA

ABSTRACT

We report the discovery of Pavo, a faint ($M_V = -10.0$), star-forming, irregular, and extremely isolated dwarf galaxy at $D \approx 2$ Mpc. Pavo was identified in Dark Energy Camera Legacy Survey imaging via a novel approach that combines low surface brightness galaxy search algorithms and machine learning candidate classifications. Follow-up imaging with the Inamori-Magellan Areal Camera & Spectrograph on the 6.5 m Magellan Baade telescope revealed a color–magnitude diagram (CMD) with an old stellar population, in addition to the young population that dominates the integrated light, and a tip-of-the-red-giant-branch distance estimate of $1.99^{+0.20}_{-0.22}$ Mpc. The blue population of stars in the CMD is consistent with the youngest stars having formed no later than 150 Myr ago. We also detected no H α emission with SOAR telescope imaging, suggesting we may be witnessing a temporary low in Pavo’s star formation. We estimate the total stellar mass of Pavo to be $\log M_*/M_\odot = 5.6 \pm 0.2$ and measure an upper limit on its H I gas mass of $1.0 \times 10^6 M_\odot$ based on the HIPASS survey. Given these properties, Pavo’s closest analog is Leo P ($D = 1.6$ Mpc), previously the only known isolated, star-forming, Local Volume dwarf galaxy in this mass range. However, Pavo appears to be even more isolated, with no other known galaxy residing within over 600 kpc. As surveys and search techniques continue to improve, we anticipate an entire population of analogous objects being detected just outside the Local Group.

Keywords: Dwarf irregular galaxies (417); Low surface brightness galaxies (940); Galaxy stellar content (621); Galaxy environments (2029); Galaxy distances (590)

1. INTRODUCTION

Galaxies at the extreme low-mass end ($M_* \lesssim 10^6 M_\odot$) of the population offer unique tests of our understanding of galaxy evolution and cosmology (e.g. Bullock &

Boylan-Kolchin 2017; Sales et al. 2022). With the rise of cosmological simulations over the past few decades, several high profile discrepancies between the number and form of low-mass galaxies in these simulations and those observed in the Local Volume came to light (Moore 1994; Klypin et al. 1999; Boylan-Kolchin et al. 2011; Pawlowski et al. 2012; McGaugh 2012). The inclusion of additional astrophysics in increasingly high resolution simulations (e.g. Brook & Di Cintio 2015; Dutton et al. 2016; Wetzel et al. 2016; Sawala et al. 2016; Garrison-

Corresponding author: Michael G. Jones
jonesmg@arizona.edu

* This paper includes data gathered with the 6.5 m Magellan Telescope at Las Campanas Observatory, Chile.

Kimmel et al. 2017) and the continued discovery of more nearby low-mass galaxies with improved surveys (e.g. Willman et al. 2005; Belokurov et al. 2006; Irwin et al. 2007; McConnachie et al. 2008; Koposov et al. 2015; Drlica-Wagner et al. 2015; Cerny et al. 2021; Collins et al. 2022), have offered resolutions to most of these issues. However, our understanding of the very lowest mass galaxies, especially beyond the influence of the Milky Way (MW) and M 31, remains quite limited. In particular, current cosmological models predict that galaxies below a certain mass threshold will be permanently quenched by cosmic reionization (Benson et al. 2002; Bovill & Ricotti 2009; Simpson et al. 2013; Wheeler et al. 2015; Fitts et al. 2017), but this characteristic mass threshold is still largely unconstrained observationally (see Simon 2019, for a review).

Resolved star searches with the Sloan Digital Sky Survey (SDSS, York et al. 2000), the Dark Energy Survey (DES, Sánchez & Des Collaboration 2010), the Dark Energy Camera Legacy Survey (DECaLS, Dey et al. 2019), and the DECam Local Volume Exploration survey (DELVE, Drlica-Wagner et al. 2021) led to a flurry of ultra-faint dwarf (UFD)¹ discoveries in (or just outside) the LG (e.g. Willman et al. 2005; Belokurov et al. 2006; Koposov et al. 2015; Drlica-Wagner et al. 2015; Sand et al. 2022; Martínez-Delgado et al. 2022; Collins et al. 2022; Cerny et al. 2023; McQuinn et al. 2023), while focused deep imaging projects identified small samples of faint dwarfs in other nearby groups (e.g. Chiboucas et al. 2013; Crnojević et al. 2014, 2016; Carlin et al. 2016; Smercina et al. 2017, 2018; Bennet et al. 2019; Müller et al. 2019; Carlin et al. 2021; Mutlu-Pakdil et al. 2022; McNanna et al. 2023). In the case of star-forming galaxies, many of the currently known lowest mass galaxies were identified through their H I emission in the Arecibo Legacy Fast ALFA (Arecibo L-band Feed Array), or ALFALFA (Giovanelli et al. 2005; Haynes et al. 2018), survey and the Study of H I In Extremely Low-mass Dwarfs (SHIELD, Cannon et al. 2011).

Isolated galaxies at the lowest masses are of particular interest as they sample one of the extremes of what constitutes a galaxy, while their isolation provides a clean environment in which to study their nature in the absence of influence from other more massive galaxies. At present, two of the lowest mass galaxies known in relative isolation are Leo P, $\log L_V/L_* = 5.7$ (Giovanelli et al. 2013; McQuinn et al. 2015a), and Tucana B, $\log L_V/L_* = 4.7$ (Sand et al. 2022), with the former

¹ Generally dwarfs fainter than $M_V = -7.7$ ($M_* \lesssim 10^5 M_\odot$) are considered to be UFDs (e.g. Simon 2019).

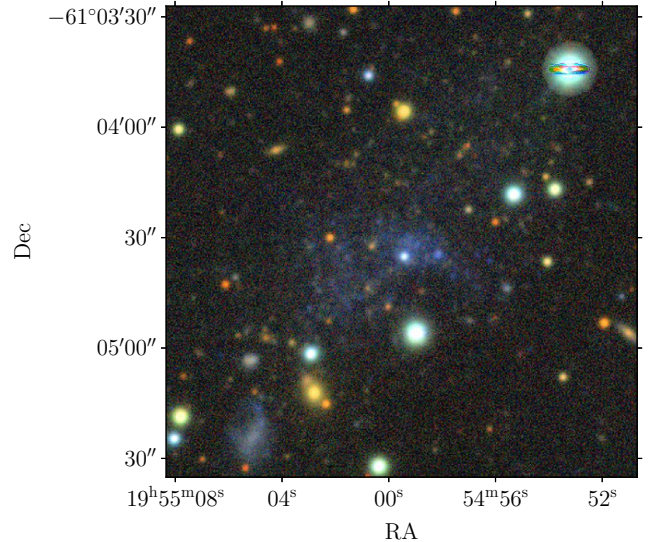


Figure 1. DECaLS DR10 *gri* cutout of Pavo, similar to that used for the original classification.

being star-forming and the latter quenched. Throughout this work we will use these two objects as points of comparison as they appear to bridge the threshold which determines whether or not a galaxy was quenched by cosmic reionization.

The stellar mass of Leo P is roughly 10 times higher than that of Tucana B (and roughly half of Leo P’s baryonic mass is in neutral gas), and in general the lowest (stellar) mass galaxies in the SHIELD sample are roughly an order of magnitude above the most massive UFDs (McQuinn et al. 2014). Thus, there is a disconnect between the lowest mass star-forming galaxies known in the field and UFDs thought to be quenched by reionization. With suitably modified search techniques and the inclusion of machine learning it is likely that existing imaging surveys can be used to begin to fill this gap and connect these two populations. There are likely many Tucana B and Leo P analogs just outside the LG, where they would appear as semi-resolved objects in existing ground-based, wide-field imaging surveys. This is a regime where current search algorithms perform poorly (e.g. Mutlu-Pakdil et al. 2021). In this letter we briefly discuss a novel approach to identifying these objects and present the first notable discovery from our search.

2. SEARCH AND DISCOVERY

Starting with publicly available images from DR10 of the Dark Energy Spectroscopic Instrument (DESI) legacy imaging surveys (Dey et al. 2019) DECaLS, the Mayall *z*-band Legacy Survey (MzLS), and the Beijing-Arizona Sky Survey (BASS), we have used a modified

version of the Systematically Measuring Ultra-Diffuse Galaxies (SMUDGes, Zaritsky et al. 2019) pipeline as well as retraining its neural network classifier to identify both UFD and SHIELD-like objects. Here we give a brief overview of the search process. Full details of the SMUDGes pipeline can be found in the original publications (Zaritsky et al. 2019, 2021, 2022, 2023) and a more complete description of our search will be presented in subsequent papers covering all candidate objects.

The original SMUDGes pipeline used the images from individual exposures, but switched to using the Legacy Survey bricks for the northern survey area. For simplicity and speed we also chose to adopt the latter strategy. The pipeline starts by identifying high surface brightness objects, subtracting them and replacing them with characteristic noise. A range of wavelet filtering scales were then used to identify candidates. Candidates must be detected in at least two bands, separated by less than $4''$. The light profiles of the initial candidates were fit with GALFIT (Peng et al. 2002, 2010), using a forced exponential profile. Using the criteria described in Zaritsky et al. (2023) several cuts were then applied: $r_e > 4''$, $b/a > 0.34$, and $\mu_{0,g} > 22.5$ mag arcsec $^{-2}$, or $\mu_{0,z} > 21.5$ mag arcsec $^{-2}$ where g -band was unavailable. These cuts were originally designed to eliminate some of the large number of spurious objects picked up by the wavelet filtering, while remaining generous enough to avoid rejecting candidates that would pass a second round of fitting with full Sérsic profiles (a more computationally intensive step). However, in practice no further cuts were needed after the second round of GALFIT fitting (with a free Sérsic index) before beginning to classify the candidates.

These steps produced a sample of approximately 4×10^5 candidates over the full Legacy Survey DR10. We began by visually inspecting all candidates within a ~ 300 deg 2 pilot area and classifying them as either candidate nearby (semi-)resolved galaxies (our target objects), other types of galaxies (not the targets of this search), or spurious detections (e.g. distant galaxy groups or Galactic cirrus). The SMUDGes convolutional neural network (CNN) image classifier was then retrained with g , r , and z fits cutouts ($\sim 88'' \times 88''$) of known UFDs, Local Volume dwarf galaxies, the nearest SHIELD galaxies, low luminosity globular clusters within the LG, and high confidence candidates from the pilot search. The spurious candidates were also added to the training set as negative examples. A second pilot area of ~ 150 deg 2 near the Galactic plane was used to test the level of contamination from Galactic cirrus. This led to a second round of training containing many examples of unwanted cirrus features.

A total of 3933 candidates were given $>90\%$ probability of being (semi-)resolved nearby galaxies by the CNN classifier, a factor of ~ 100 reduction from the initial catalog of candidates.² After an initial visual screening for spurious candidates that made it past the CNN (mostly cirrus, background galaxy groups, spiral arms, or tidal structures), cutouts of 1314 candidates were uploaded to the Zooniverse platform³ where six volunteers from our team classified them as in the pilot search discussed above. A total of 321 of these candidates were classified by a least one volunteer as likely being a nearby, low-mass (semi-)resolved galaxy and therefore flagged for further investigation. The majority of these objects are known nearby galaxies, however, roughly a quarter are entirely uncatalogued.

One striking example is shown in Figure 1: a blue, irregular dwarf galaxy reminiscent of Leo P. Upon inspection, it was immediately realized that this is likely a very nearby object due to its extended and clearly semi-resolved appearance in the ground-based DECaLS imaging. We named this object ‘‘Pavo’’ after the constellation in which it resides.

3. FOLLOW-UP OBSERVATIONS

3.1. Magellan Baade imaging

To further understand the physical and star formation properties of Pavo, we obtained deep g and r -band imaging with the Inamori-Magellan Areal Camera & Spectrograph (IMACS; Dressler et al. 2006) on the Magellan Baade 6.5-m telescope on 2023 July 14 (UT). We used the $f/2$ camera, which has a $\sim 27.4'$ field of view and 0.2 arcsec/pixel scale. We took 11×300 s exposures in the g -band and 11×300 s exposures in the r -band, with small dithers in between exposures. The data were reduced in a standard way (as in Chiti et al. 2020) with standard image detrending. Astrometric correction was a two-step process, with an initial world coordinate system solution supplied by `astrometry.net` (Lang et al. 2010), followed by a refined solution computed by SCAMP (Bertin 2006). Final image stacking used the SWarp (Bertin et al. 2002) software package, using a weighted average of the input images. The final, stacked images have point spread function full-width half maximum (FWHM) values of $0.9''$ in both the g and r bands.

² In the case of MzLS/BASS we performed Gaussian smoothing with a 1.5 pixel kernel to reduce noise before passing the candidate cutouts to the CNN. A threshold probability of 98% was also used for MzLS/BASS (instead of 90%) to reduce the number of false positive candidates.

³ www.zooniverse.org

Point source photometry was performed on the stacked IMACS images using the `daophot` and `allframe` software suite (Stetson 1987, 1994), similar to that described in Mutlu-Pakdil et al. (2018). We removed objects that are not point sources by culling our `allframe` catalog of outliers in χ^4 versus magnitude, magnitude error versus magnitude, and sharpness versus magnitude space. We calibrated the photometry by matching it to the Legacy Survey DR10. We corrected for MW extinction on a star-by-star basis using the Schlegel et al. (1998) reddening maps with the coefficients from Schlafly & Finkbeiner (2011). The extinction-corrected photometry is used throughout this work.

We perform a series of artificial star tests with the `daophot` routine `addstar` to determine our photometric errors and completeness as a function of magnitude and color. Similar to Mutlu-Pakdil et al. (2018), we placed artificial stars into our images on a regular grid (10–20 times the image FWHM). Ten iterations are performed on the image for a total of $\sim 100,000$ artificial stars each. These images are then photometered in the same way as the unaltered image stacks and the same stellar selection criteria on χ , magnitude, magnitude error, and sharpness were applied to the artificial star catalogs to determine completeness and magnitude uncertainties. The 50% (90%) completeness level is at $r = 26.5$ (24.5) and $g = 27.0$ (24.5) mag.

3.2. SOAR H α imaging

To look for sites of ongoing star formation, an H α image of Pavo was obtained with the 4.1 m Southern Astrophysical Research (SOAR) telescope on 2023 September 17 with the Goodman Spectrograph (Clemens et al. 2004). The narrow band H α filter has a central wavelength of 6563 Å and a width of 75 Å. The SDSS r -band filter was used for the continuum image. Pavo was observed with a 3-point dither in both filters for total exposure times of 1800 s (H α) and 180 s (r). Images were binned 2×2 to give a pixel scale of 0.3 arcsec/pixel.

Images were reduced using `ccdproc`. Individual exposures were aligned with `astroalign` before median stacking, and the final world coordinate system was derived with `astrometry.net`. Stars were extracted from both the r -band and H α images and a linear fit to the relation between their fluxes was used to scale the r -band image and subtract the continuum. The continuum subtraction removed the entirety of Pavo from the H α image, indicating that there are no sites of significant H α emission (i.e. H II regions).

⁴ χ is a measure of the quality of the fit between the model and the actual stars in the image.

Table 1. Properties of Pavo

Parameter	Value
RA	19:54:59.98 \pm 7.9''
Dec.	−61:04:20.5 \pm 5.8''
m_g /mag	16.7 \pm 0.1
m_r /mag	16.4 \pm 0.1
m_i /mag	16.3 \pm 0.1
m_z /mag	16.1 \pm 0.1
Dist./Mpc	1.99 ^{+0.20} _{−0.22}
M_V /mag	−10.0 \pm 0.1
r_h	1.25' \pm 0.10'
r_h /pc	713 \pm 57
ϵ	0.51 \pm 0.08
θ	131° \pm 21°
log(SFR _{UV} /M _⊙ yr ^{−1})	−4.0 ^{+0.3} _{−0.8}
log M_*/M_\odot	5.6 \pm 0.2
log M_{HI}/M_\odot	< 6.0

NOTE—Stated uncertainties of distance-dependent quantities do not include the contribution from the distance uncertainty.

3.3. Swift observations

Pavo lies in a gap in the Galaxy Evolution Explorer (GALEX) all-sky imaging survey and we therefore obtained UV imaging from the NASA Neil Gehrels Swift observatory in all three UV bands (UVW1, UVM2, UVW2). Pavo was observed over two sequences on 2023 September 19 and 20. Unfortunately, the sequence taken on 2023 September 19 was unusable due to a detector artifact produced by a bright star, leaving only the 2023 September 20 sequence. Pavo was detected in all three bands, however, due to its color similarity to GALEX NUV we use only the UVM2 filter to determine star formation rate (Hoversten et al. 2009). We measure the flux from Pavo using an aperture based on double the optical half light radius, masking contaminating sources such as bright stars in this region. The measured flux is very close to the zero point for the Ultra-Violet Optical Telescope (UVOT) and therefore the uncertainty on the measured flux is high. The raw flux was corrected for foreground extinction and sensitivity loss following the UVOT calibration documents. We then color correct the UVOT flux to GALEX NUV and use the relation from Iglesias-Páramo et al. (2006) to derive a star formation rate (Table 1).

4. PROPERTIES OF PAVO

4.1. Color and morphology

The DECaLS image of Pavo is dominated by its young, blue stellar component, which extends from the

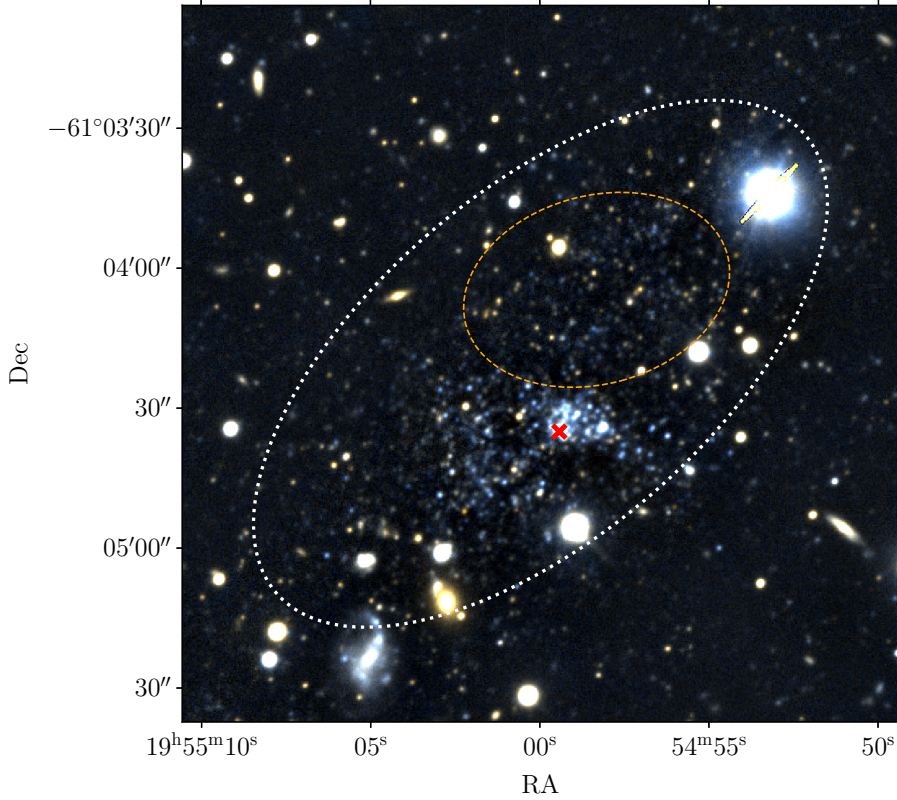


Figure 2. IMACS $g + r$ color image of Pavo. The central and SE portions of its irregular stellar body are dominated by blue stars, but it also extends to the NW where older, redder stars become the dominant population. The white dotted ellipse shows the region used to produce the full CMD of Pavo (Figure 3, top-left) and the orange dashed ellipse shows the region dominated by redder stars (Figure 3, top-right). The field contains many foreground stars, and the apparent central cluster of Pavo is actually a superimposed foreground star with detectable proper motion. We have marked this star with a red x.

center of Figure 1 to the SE. It has a highly speckled appearance indicating that the stellar population is only slightly too distant to be resolved into individual stars. The distribution of blue stars is also highly irregular, with no clear ordered structure or center. Prior to the SOAR $H\alpha$ observations (and the non-detection of Pavo), the brightest clump near the center of the image was considered as a possible star cluster or $H\text{ II}$ region. However, this object was identified as having measurable proper motion (7.2 mas/yr) in the Gaia survey (Gaia Collaboration et al. 2016, 2023), and is therefore a foreground star. Bailer-Jones et al. (2021) estimate the distance to this star as $3.0^{+1.5}_{-1.0}$ kpc. It is marked with a red x in Figure 2.

The IMACS image of Pavo (Figure 2) resolves the stellar population, revealing that, in addition to the blue stars seen in the DECaLS image in the SE, an older, redder population extends to the NW. This is likely the underlying stellar population of the galaxy, whereas the seemingly dominant blue population only represents the most recent star formation. Star formation is highly stochastic in low-mass galaxies (e.g. McQuinn et al.

2015b), thus the blue population that dominates the total integrated light can give a very misleading impression of the underlying structure (cf. §4.3).

These findings indicate that Pavo hosts both an old stellar population and a recently formed one. It therefore cannot be a transient object, and instead is a long-lived, bona fide dwarf galaxy, albeit at a very low mass. It must also have recently contained enough gas to ignite a recent episode of star formation. It may have been continuously forming stars (perhaps with bursts and lulls) for much of its lifetime, or it may have only recently begun to form stars again after a long quiescent period. We will revisit this point and discuss the nature of its stellar population in §4.4.

4.2. Distance

We derive the distance to Pavo via the tip of the red giant branch (TRGB) method (e.g., Da Costa & Armandroff 1990; Lee et al. 1993; Makarov et al. 2006), where the sharp discontinuity at the bright end of an old red giant branch (RGB) population is used as a standard candle. To perform the measurement, we only consider the NW region of the galaxy (see Figure 3), in

order to have as little contamination as possible from the young, massive stars in Pavo; we additionally apply a color cut of $g - r < 1.35$ to avoid foreground contaminants. We derive the luminosity function for the RGB stars, and fit it with a model luminosity function, after having convolved the latter with the photometric uncertainty, bias, and completeness as derived from our artificial star tests (see Crnojević et al. 2019 for details). The nonlinear least-square fitting returns a value of $r_{\text{TRGB}} = 23.48 \pm 0.21$ for the TRGB magnitude. This translates into a distance modulus of $(m - M) = 26.49 \pm 0.23$ mag, or a distance of $1.99^{+0.20}_{-0.22}$ Mpc, according to the TRGB calibration in SDSS bands derived by Sand et al. (2014), $M_r^{\text{TRGB}} = -3.01 \pm 0.10$. An old, metal-poor RGB isochrone from the PAdova and TRieste Stellar Evolution Code (PARSEC, Bressan et al. 2012), scaled to this distance, is overlaid on a binned version of the CMD in the bottom central panel of Figure 3.

4.3. Structural Parameters

To measure the underlying structural parameters of Pavo, we fit an exponential profile to the two-dimensional distribution of stars consistent with the RGB using a maximum likelihood technique (Martin et al. 2008), as implemented in Sand et al. (2012). We selected RGB stars using a color–magnitude selection region within 2σ (photometric uncertainties) of an ancient (10 Gyr) and very metal-poor ($[M/H] = -2.5$) PARSEC RGB isochrone. This isochrone is shown in orange in most panels of Figure 3. The top-right panel shows stars from the NW region of Pavo (orange dotted ellipse in Figure 2) compared to this isochrone. Applying this photometric selection across the whole IMACS field yielded our input RGB catalog for our structural analysis. Only stars brighter than $r=26.5$ mag were included in our selection.

The exponential profile fit includes the central position, position angle (θ), ellipticity (ϵ), half-light radius (r_h), and a constant background surface density as free parameters. The algorithm accounts for saturated foreground stars and other regions where Pavo stars could not be detected. Uncertainties were calculated through a bootstrap resampling analysis, using 1000 iterations. As a check, we also repeated the calculations while only including RGB stars down to $r=25.5$ mag; the derived structural parameters agreed within the uncertainties.

The results of the structural analysis can be seen in Table 1 and Pavo is placed on the size–luminosity relation for dwarf galaxies in Figure 4. Pavo is a close match in luminosity to both Leo P and the gas-rich dwarf Antlia B (Sand et al. 2015), but is several times

larger. However, all three dwarfs still fall within the scatter of the size–luminosity relation of LG dwarfs.

4.4. Stellar population

To investigate the red and blue stellar populations in Pavo further, we selected blue stars to contrast with the RGB population from §4.3. To do this we adopted a simple selection criterion of $g - r < 0$. The positions of the red and blue populations are plotted in Figure 5. In both cases we plot only stars brighter than $m_r = 26$. There are holes in the distribution of stars in certain places due to bright foreground stars or background galaxies. The former are highlighted in Figure 5 with grey circles. For the latter, we simply note that the largest gaps are in the lower-left (SE) of Figure 5 due to bright background early-type and late-type galaxies (cf. Figure 2).

From Figure 5 we can clearly see that the NW side of Pavo is dominated by RGB stars, while the south is dominated by blue stars. In both cases there is a clear overdensity of stars relative to the background and the majority of this overdensity is encompassed by the ellipse in Figure 5 that was also used to produce the CMD in Figure 3 (top-left).

As discussed in §4.2, the red stellar population in the NW of Pavo is consistent with being an ancient metal-poor RGB at ~ 2 Mpc. This is seen even more clearly in the Hess diagram (with 0.1 mag bins) in Figure 3 (bottom-center) where the RGB isochrone follows the densest parts of the CMD, while overlapping an underdensity in the background CMD (bottom-right).

We briefly considered the possibility that this red population might instead be merely the red side of the Helium-burning (HeB) branch, with the blue population being the blue side of the branch (and the top of the main sequence of the youngest stars). However, the fact that the two populations can be spatially separated (e.g. Figures 5 & 3, top-right) refutes this notion. In addition, a relatively high metallicity (for an object of this luminosity) $[M/H] \approx -1$ would be required to match the observed colors of the two populations.

In the case of the blue population, the isochrones in Figure 3 (top left) indicate that it is consistent with a combination of main sequence and HeB stars that are 150–500 Myr old (at 2 Mpc). The metallicity for these isochrones was chosen to approximately match that of Leo P as we currently have no metallicity estimate for Pavo. The CMD therefore indicates that there was some star formation at least as recently as 150 Myr ago, however, when considering the brightest and bluest stars we are dealing with small number statistics and it is possible that Pavo contains some younger stars.

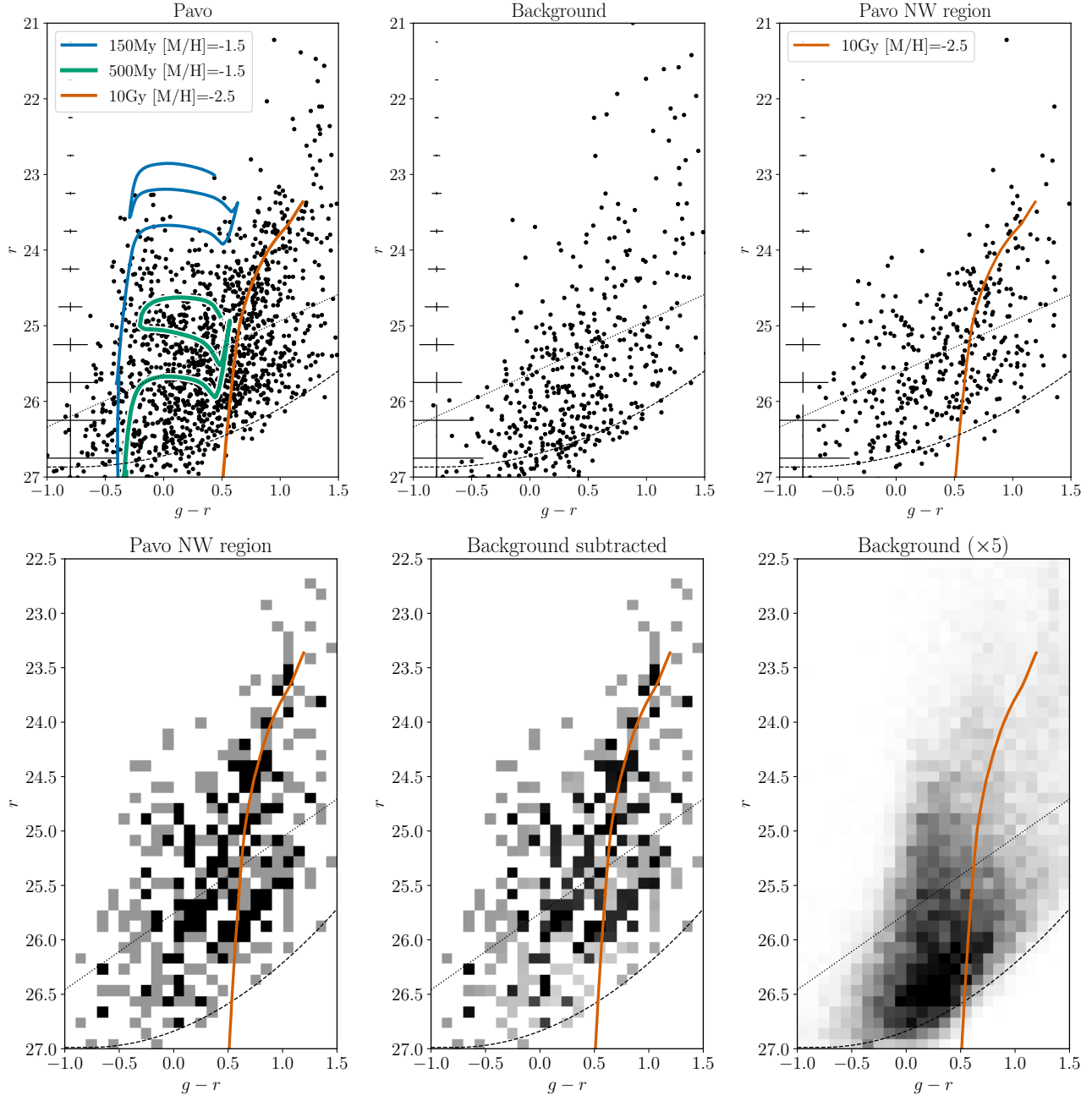


Figure 3. *Top-left:* Color magnitude diagram (CMD) of the stellar population of Pavo from the IMACS imaging. The blue and green isochrones indicate the main sequence and helium burning phases of 150 Myr and 500 Myr old populations, respectively. The metallicity in both cases is set to $[M/H] = -1.5$ to roughly match that of Leo P. The orange isochrone shows the location of an ancient and metal-poor (10 Gyr and $[M/H] = -2.5$) RGB. *Top-center:* Background CMD created by downsampling the CMD of the full FoV (minus the region containing Pavo) to an area equal to the white dashed ellipse in Figure 2. *Top-right:* CMD of the stellar population within the orange dotted ellipse (Figure 2). The RGB isochrone from the left panel is reproduced here. In all three panels (top) the dashed line indicates the 50% completeness limit and the dotted line the 90% limit, and the error bars on the left indicate the typical photometric uncertainties in bins of 0.5 mag in r -band. *Bottom-left:* Binned version of the CMD of the NW region of Pavo (0.1 mag bins). *Bottom-center:* The same CMD with the background contribution subtracted. *Bottom-right:* Binned CMD of the background over the entire FoV (with Pavo excluded), weighted by five times the area of the region used in the bottom-left and bottom-center CMDs (to make it more clearly visible on the same scale). The 10 Gyr, $[M/H] = -2.5$ PARSEC isochrone (at a distance of 1.99 Mpc) is overlaid in orange.

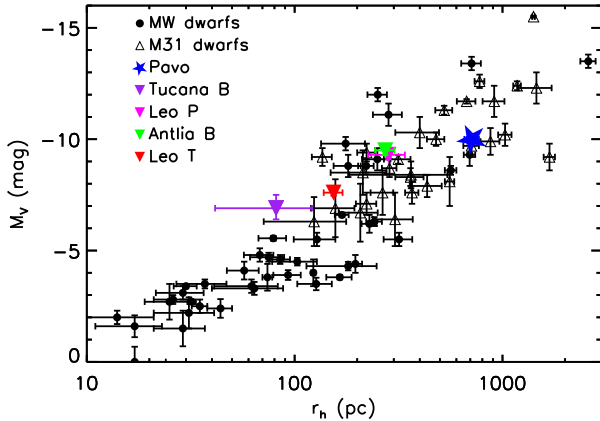


Figure 4. Pavo on the size–luminosity relation with various other Local Volume dwarfs included for comparison. Note that Pavo is at the upper limit of the scatter in effective radius (for its magnitude), while all of the highlighted comparison dwarfs are at the lower limit of the scatter.

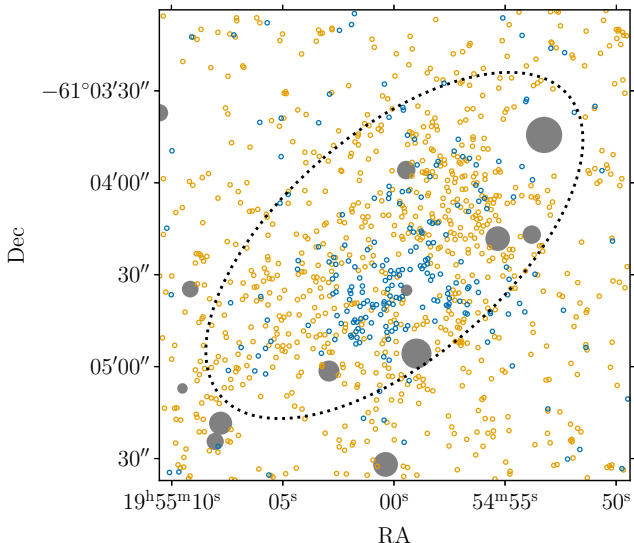


Figure 5. Map of the positions of blue, $g - r < 0$ (blue points), and RGB (orange points) stars (both) brighter than $m_r = 26$. The grey points show the locations of bright stars from Gaia DR3 ($m_G < 19.5$) with point sizes scaled by apparent brightness. The dashed black ellipse indicates the half-light radius of Pavo (Table 1). It is the same ellipse as in Figure 2.

Our $H\alpha$ observations (§3.2) revealed no H II regions, also supporting the notion that there are no very young stars (< 10 Myr). However, we note that this does not mean Pavo has completely stopped forming stars. Star formation in these extremely low mass galaxies is highly stochastic and will not evenly sample the full initial mass function at any given time. It may be possible that

new stars have formed in the past 10 Myr, but none of them are O stars and thus there are no H II regions. For comparison, Leo P has a single H II region that probably contains only a single O star (Rhode et al. 2013).

To assess this more quantitatively we consider that the Swift UV detection of Pavo indicates that over the past ~ 200 Myr it has had an average SFR of $\sim 1 \times 10^{-4} M_{\odot} \text{ yr}^{-1}$. Assuming this SFR, Pavo might have formed $1000 M_{\odot}$ of stars in the past 10 Myr. We used PARSEC to generate 800 realizations of a $1000 M_{\odot}$, 10 Myr old single stellar population (with a Kroupa initial mass function, IMF). Every realization contained at least one O star, suggesting that the lack of $H\alpha$ emission, even at these low masses, does imply that there has been a cessation of star formation for at least the past 10 Myr. Another possibility is that the IMF may be top-light, which has been suggested is expected for metal-poor systems with low SFRs (Pflamm-Altenburg & Kroupa 2009; Jeřábková et al. 2018). If this were the case for Pavo then it is possible that star formation is still proceeding but there are no stars massive enough to form H II regions. Overall, the simplest explanation is likely that star formation in Pavo proceeds quasi-episodically and we are currently witnessing a temporary low.

Space-based observations of Pavo will have the depth and resolution to better resolve its stellar population. This will provide considerably more information on the recent star formation, revealing if Pavo has indeed been forming stars in episodic bursts or if its SFR has been largely steady. This will give a clearer indication of whether we are witnessing a temporary lull in SFR, or the beginning of a permanent shutdown.

4.5. Stellar and gas masses

To estimate the stellar mass of Pavo we performed aperture photometry (Table 1) on the DECaLS g , r , z , and i , masking clear foreground stars. The stellar mass was estimated using five different magnitude and color scaling relations (based on r and i -band magnitudes and $g - r$ and $g - i$ colors) from Zibetti et al. (2009), Taylor et al. (2011), and Du & McGaugh (2020). The median value $\log M_{*}/M_{\odot} = 5.6$ was adopted as our stellar mass estimate and the standard deviation between the five methods, 0.2 dex, used as the uncertainty (note this does not include distance uncertainty). This mass is identical within the uncertainty to that of Leo P, $\log M_{*}/M_{\odot} = 5.7$ (McQuinn et al. 2015a).

We extracted an H I spectrum at the position of Pavo from the H I Parkes All Sky Survey (HIPASS, Barnes

et al. 2001) spectral server⁵, but could not identify any significant emission peaks that might correspond to its neutral gas content. There is a $\sim 2\sigma$ peak at approximately $cz_{\odot} = 1000 \text{ km s}^{-1}$, however, unless Pavo has a particularly large peculiar velocity (e.g. $>500 \text{ km s}^{-1}$) it is unlikely that this peak, if real, is associated. It is also possible that the velocity of Pavo is sufficiently small that any H I emission is overwhelmed by that of the MW. Without dismissing this possibility, if we assume that Pavo’s radial velocity is sufficiently large to not be blended with the H I emission of the MW (e.g. $cz_{\odot} \gtrsim 100 \text{ km s}^{-1}$, for this region of the sky), we can estimate an upper limit for its H I mass based on the HIPASS spectrum. This spectrum has an rms noise of 8.2 mJy (13 km s^{-1} resolution). If we assume a velocity width of 30 km s^{-1} for Pavo (Leo P’s H I velocity width is 24 km s^{-1} , Giovanelli et al. 2013), then at 2 Mpc this translates to a 3σ upper limit on Pavo’s H I mass of $\log M_{\text{HI}}/M_{\odot} < 6.0$. We note that the H I mass of Leo P, $\log M_{*}/M_{\odot} = 5.9$ (Giovanelli et al. 2013; McQuinn et al. 2015a), would be marginally below this limit.

If we go further and assume that the radial velocity of Pavo is in the range 100-500 km/s, we can also use the Galactic All-Sky Survey (GASS, McClure-Griffiths et al. 2009; Kalberla & Haud 2015) to constrain Pavo’s H I mass. We inspected a spectral cube from GASS,⁶ but found no sign of H I line emission from Pavo. The rms noise in this cube was 49 mK at 1 km s^{-1} resolution. Using 0.7 K/Jy as the approximate gain of the Parkes radio telescope, this translates to a 3σ upper limit on the H I mass of Pavo of $\log M_{\text{HI}}/M_{\odot} < 5.6$. Although this limit is slightly lower than that from HIPASS, the previous limit is stricter in the sense that it does not assume an upper limit of 500 km s^{-1} for the radial velocity of Pavo.

Although it is unclear if Pavo currently contains a significant gas reservoir it must have done recently in order to explain its population of young stars. Giovanelli & Haynes (2015) suggested that very low-mass, star-forming galaxies, such as Pavo and Leo P, might periodically become invisible to H I surveys if feedback ejects much of their gas reservoirs. Recent simulations of galaxies in this mass range (Rey et al. 2020, 2022) support this hypothesis. Thus, it may be that Pavo’s apparent lull in SFR is also reflected in its gas content. However, deeper H I observations are needed to confirm/refute this possibility.

4.6. Environment

⁵ <https://www.atnf.csiro.au/research/multibeam//release/>

⁶ <https://www.astro.uni-bonn.de/hisurvey/gass/index.php>

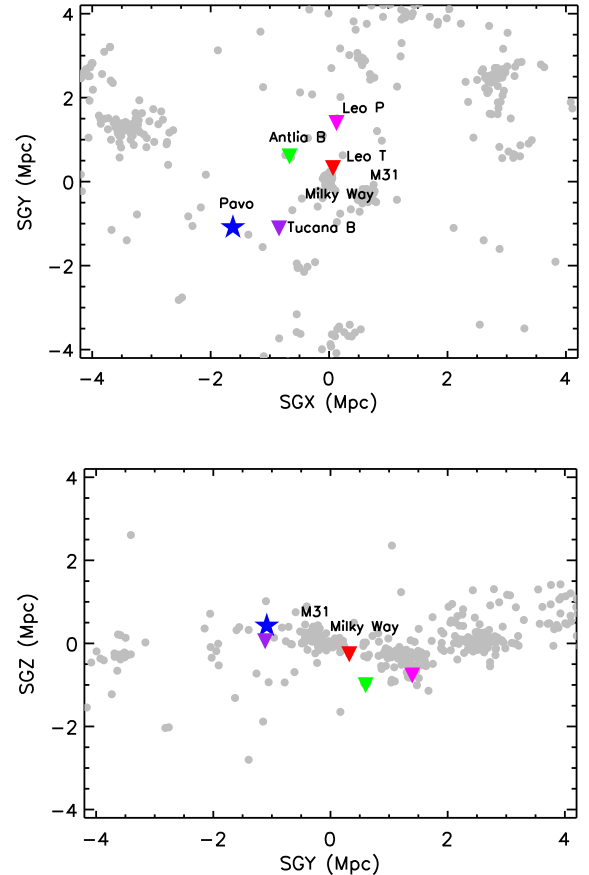


Figure 6. Supergalactic XY (top) and YZ (bottom) projections showing objects in the nearby galaxies catalog (Karachentsev & Kaisina 2019). Pavo is shown with a blue star. Several other notable dwarf galaxies which we refer to are highlighted for comparison.

Figure 6 shows two projections (in Cartesian supergalactic coordinates) of nearby galaxies (from Karachentsev & Kaisina 2019). We have highlighted Pavo as well as Tucana B and Leo P for the purpose of comparison. Pavo is slightly further from the MW than either Tucana B or Leo P, and in fact is remarkably isolated. The two panels of Figure 6 show that Pavo is part of the local sheet and is in a direction away from any known nearby group/structure. In 3-dimensions the nearest neighbor to Pavo (in the catalog of Karachentsev & Kaisina 2019) is IC 5152 over 600 kpc away. This makes it even more isolated than Leo P, which is already regarded as a pristine object that likely has never entered the virial radius of a more massive system (Giovanelli et al. 2013).

5. DISCUSSION

The exceptional isolation of Pavo makes it an ideal candidate for follow-up observations to understand how

star formation proceeds in the lowest mass star-forming galaxies. Upcoming space-based observations (HST-GO-17514; PI: B. Mutlu-Pakdil) will be capable of resolving its stellar population, even in the brightest clumps where our IMACS data become too crowded (Figure 5), and trace both the main sequence and RGB down to fainter magnitudes. Fitting star formation histories to these deeper CMDs (cf. McQuinn et al. 2015b) would indicate whether Pavo has been continuously forming stars since before reionization, formed stars episodically, or perhaps only recently revived its star formation after having been quenched at high redshift.

Although we have compared Pavo to Leo P and Tucana B throughout this work, we note that really there is no other known galaxy that is a close match for all of Pavo’s properties. Tucana B is clearly not morphologically similar to Pavo, but we used it as a point of comparison because Tucana B is currently the only known isolated UFD. Presumably, if Pavo were several times less massive, its gas reservoir would not have survived reionization, and today it would appear more like Tucana B. Pavo and Leo P are morphologically similar and appear to have similar stellar populations, but the spatial extent of Pavo’s RGB stars is roughly five times larger than that of Leo P’s, indicating that it is quite a different object. The close similarity of the physical properties of Antlia B and Leo P (e.g. Figure 4), while one is close to a massive galaxy and the other is isolated, suggests that relative isolation is unlikely to be the root cause of Pavo’s more extended stellar population, and that instead there is probably an underlying, intrinsic cause. Really what the lack of close comparisons for Pavo highlights is the dearth of isolated galaxies that are known in this mass regime. Building a better understanding of these objects and determining observationally where the tipping point between objects like Pavo and Tucana B occurs will require a statistical sample of isolated dwarfs (both quenched and star-forming) in this mass regime ($M_* \lesssim 10^6 M_\odot$).

Exceptionally low mass, star-forming galaxies such as Pavo and Leo P trace the boundary of galaxy mass needed to survive cosmic reionization and continue forming stars. Tollerud & Peek (2018) used the transitional dwarf Leo T, $\log L_V/L_\odot = 5.1$ and $D = 0.42$ Mpc (Irwin et al. 2007), to place an approximate upper limit on this mass scale. However, just above the mass of Leo T there should be an abundance of Leo P analogs just outside the LG. We posit that Pavo is merely the first such analog to be identified. By building up this sample, as well as a sample of field UFDs (e.g. Tucana B analogs), we can constrain the mass threshold to survive

reionization from both sides, without the complication of interactions with a host galaxy.

In the next few years new wide-field HI surveys, currently in progress, will undoubtedly uncover new analogous star-forming dwarfs. In particular, the Commensal Radio Astronomy FasT Survey (CRAFTS, Zhang et al. 2021) with the Five hundred meter Aperture Spherical Telescope (FAST) and the Widefield ASKAP (Australia Square Kilometre Array Pathfinder) L-band Legacy All-sky Blind survey (WALLABY, Koribalski et al. 2020), will together cover almost the entire sky to at least the sensitivity of ALFALFA (several times deeper than HIPASS). These HI surveys will pick out any Leo P analogs and, at slightly higher masses, will greatly expand on the SHIELD sample. However, as these surveys will only be sensitive to gas-bearing galaxies that have fuel for star formation (and that therefore likely contain young, blue stars), many of the objects that they will uncover in this regime are likely already identifiable in Legacy Survey images, if they are searched for with a suitably optimized approach. Pavo may be the first such object to have been identified, but there are undoubtedly many more.

At optical and infra-red wavelengths the upcoming Rubin Legacy Survey of Space and Time (LSST) and the Nancy Grace Roman High Latitude Wide Area Survey will provide unprecedented opportunities to identify nearby, isolated and very low mass dwarf galaxies. Resolved star searches will be an effective tool with LSST out to a few Mpc (e.g. Mutlu-Pakdil et al. 2021), while for Roman this technique will be viable out to ~ 10 Mpc (but over a much smaller survey area). However, as our discovery of Pavo has demonstrated, this distance range can readily be extended by incorporating machine learning-aided classification in the semi-resolved regime. As the accessible survey volume grows like the cube of distance, even increasing this maximum distance by a small factor represents a major gain in terms of the number of identifiable sources.

In subsequent papers, we will present the full sample of candidate analogs to Leo P, SHIELD galaxies, and Tucana B that we have uncovered in our machine learning-aided search of the DESI legacy imaging surveys. Further developing and optimizing this technique will allow semi-resolved nearby dwarf galaxies to be identified not just in existing imaging surveys, but also in upcoming next-generation surveys, such as LSST and Roman, and maximize their potential for extra-galactic science at the lowest masses.

We thank the anonymous referee for their rapid and helpful response. This work used images from the Dark Energy Camera Legacy Survey (DECaLS; Proposal ID 2014B-0404; PIs: David Schlegel and Arjun Dey). Full acknowledgment at <https://www.legacysurvey.org/acknowledgment/>. Based on observations obtained at the Southern Astrophysical Research (SOAR) telescope, which is a joint project of the Ministério da Ciência, Tecnologia e Inovações (MCTI/LNA) do Brasil, the US National Science Foundation's NOIRLab, the University of North Carolina at Chapel Hill (UNC), and Michigan State University (MSU). This publication uses data generated via the [Zooniverse.org](https://www.zooniverse.org) platform, development of which is funded by generous support, including a Global Impact Award from Google, and by a grant from the Alfred P. Sloan Foundation. DJS acknowledges support from NSF grants AST-1821967, 1813708 and AST-2205863. Research by DC is supported by NSF grant AST-1814208. KS acknowledges support from the Natural Sciences and Engineering Research Council of Canada (NSERC). JS acknowledges support from the Packard Foundation. AK acknowledges support from NSERC, the University of Toronto Arts & Science Postdoctoral Fellowship program, and the Dunlap Institute. DZ and RD acknowledge support from NSF AST-2006785 and NASA ADAP 80NSSC23K0471 for their work on the SMUDGes pipeline.

Facilities: Blanco, Magellan:Baade (IMACS), SOAR, Swift, Parkes, Gaia

Software: [astrometry.net](#) (Lang et al. 2010), [SCAMP](#) (Bertin 2006), [SWarp](#) (Bertin et al. 2002), [astropy](#) (Astropy Collaboration et al. 2013, 2018), [Photutils](#) (Bradley et al. 2020), [reproject](#) (Robitaille et al. 2020), [matplotlib](#) (Hunter 2007), [numpy](#) (van der Walt et al. 2011), [scipy](#) (Oliphant 2007; Millman & Aivazis 2011), [pandas](#) (Wes McKinney 2010; pandas development team 2020), [astroquery](#) (Ginsburg et al. 2019), [astroalign](#) (Beroiz et al. 2020), [ccdproc](#) (Craig et al. 2017), [DS9](#) (Joye & Mandel 2003), [GALFIT](#) (Peng et al. 2002, 2010), [daophot](#) and [allframe](#) (Stetson 1987, 1994)

REFERENCES

- Astropy Collaboration, Robitaille, T. P., Tollerud, E. J., et al. 2013, *A&A*, 558, A33, doi: [10.1051/0004-6361/201322068](https://doi.org/10.1051/0004-6361/201322068)
- Astropy Collaboration, Price-Whelan, A. M., Sipőcz, B. M., et al. 2018, *AJ*, 156, 123, doi: [10.3847/1538-3881/aabc4f](https://doi.org/10.3847/1538-3881/aabc4f)
- Bailer-Jones, C. A. L., Rybizki, J., Fouesneau, M., Demleitner, M., & Andrae, R. 2021, *AJ*, 161, 147, doi: [10.3847/1538-3881/abd806](https://doi.org/10.3847/1538-3881/abd806)
- Barnes, D. G., Staveley-Smith, L., de Blok, W. J. G., et al. 2001, *MNRAS*, 322, 486, doi: [10.1046/j.1365-8711.2001.04102.x](https://doi.org/10.1046/j.1365-8711.2001.04102.x)
- Belokurov, V., Zucker, D. B., Evans, N. W., et al. 2006, *ApJL*, 647, L111, doi: [10.1086/507324](https://doi.org/10.1086/507324)
- Bennet, P., Sand, D. J., Crnojević, D., et al. 2019, *ApJ*, 885, 153, doi: [10.3847/1538-4357/ab46ab](https://doi.org/10.3847/1538-4357/ab46ab)
- Benson, A. J., Frenk, C. S., Lacey, C. G., Baugh, C. M., & Cole, S. 2002, *MNRAS*, 333, 177, doi: [10.1046/j.1365-8711.2002.05388.x](https://doi.org/10.1046/j.1365-8711.2002.05388.x)
- Beroiz, M., Cabral, J., & Sanchez, B. 2020, *Astronomy and Computing*, 32, 100384, doi: <https://doi.org/10.1016/j.ascom.2020.100384>
- Bertin, E. 2006, in *Astronomical Society of the Pacific Conference Series*, Vol. 351, *Astronomical Data Analysis Software and Systems XV*, ed. C. Gabriel, C. Arviset, D. Ponz, & S. Enrique, 112
- Bertin, E., Mellier, Y., Radovich, M., et al. 2002, in *Astronomical Society of the Pacific Conference Series*, Vol. 281, *Astronomical Data Analysis Software and Systems XI*, ed. D. A. Bohlender, D. Durand, & T. H. Handley, 228
- Bovill, M. S., & Ricotti, M. 2009, *ApJ*, 693, 1859, doi: [10.1088/0004-637X/693/2/1859](https://doi.org/10.1088/0004-637X/693/2/1859)
- Boylan-Kolchin, M., Bullock, J. S., & Kaplinghat, M. 2011, *MNRAS*, 415, L40, doi: [10.1111/j.1745-3933.2011.01074.x](https://doi.org/10.1111/j.1745-3933.2011.01074.x)
- Bradley, L., Sipőcz, B., Robitaille, T., et al. 2020, *astropy/photutils*: 1.0.0, 1.0.0, Zenodo, doi: [10.5281/zenodo.4044744](https://doi.org/10.5281/zenodo.4044744)
- Bressan, A., Marigo, P., Girardi, L., et al. 2012, *MNRAS*, 427, 127, doi: [10.1111/j.1365-2966.2012.21948.x](https://doi.org/10.1111/j.1365-2966.2012.21948.x)
- Brook, C. B., & Di Cintio, A. 2015, *MNRAS*, 450, 3920, doi: [10.1093/mnras/stv864](https://doi.org/10.1093/mnras/stv864)

- Bullock, J. S., & Boylan-Kolchin, M. 2017, *ARA&A*, 55, 343, doi: [10.1146/annurev-astro-091916-055313](https://doi.org/10.1146/annurev-astro-091916-055313)
- Cannon, J. M., Giovanelli, R., Haynes, M. P., et al. 2011, *ApJL*, 739, L22, doi: [10.1088/2041-8205/739/1/L22](https://doi.org/10.1088/2041-8205/739/1/L22)
- Carlin, J. L., Sand, D. J., Price, P., et al. 2016, *ApJL*, 828, L5, doi: [10.3847/2041-8205/828/1/L5](https://doi.org/10.3847/2041-8205/828/1/L5)
- Carlin, J. L., Mutlu-Pakdil, B., Crnojević, D., et al. 2021, *ApJ*, 909, 211, doi: [10.3847/1538-4357/abe040](https://doi.org/10.3847/1538-4357/abe040)
- Cerny, W., Pace, A. B., Drlica-Wagner, A., et al. 2021, *ApJL*, 920, L44, doi: [10.3847/2041-8213/ac2d9a](https://doi.org/10.3847/2041-8213/ac2d9a)
- Cerny, W., Martínez-Vázquez, C. E., Drlica-Wagner, A., et al. 2023, *ApJ*, 953, 1, doi: [10.3847/1538-4357/acdd78](https://doi.org/10.3847/1538-4357/acdd78)
- Chiboucas, K., Jacobs, B. A., Tully, R. B., & Karachentsev, I. D. 2013, *AJ*, 146, 126, doi: [10.1088/0004-6256/146/5/126](https://doi.org/10.1088/0004-6256/146/5/126)
- Chiti, A., Frebel, A., Jerjen, H., Kim, D., & Norris, J. E. 2020, *ApJ*, 891, 8, doi: [10.3847/1538-4357/ab6d72](https://doi.org/10.3847/1538-4357/ab6d72)
- Clemens, J. C., Crain, J. A., & Anderson, R. 2004, in *Society of Photo-Optical Instrumentation Engineers (SPIE) Conference Series*, Vol. 5492, *Ground-based Instrumentation for Astronomy*, ed. A. F. M. Moorwood & M. Iye, 331–340, doi: [10.1117/12.550069](https://doi.org/10.1117/12.550069)
- Collins, M. L. M., Charles, E. J. E., Martínez-Delgado, D., et al. 2022, *MNRAS*, 515, L72, doi: [10.1093/mnrasl/slac063](https://doi.org/10.1093/mnrasl/slac063)
- Craig, M., Crawford, S., Seifert, M., et al. 2017, *astropy/ccdproc: v1.3.0.post1, v1.3.0.post1*, Zenodo, doi: [10.5281/zenodo.1069648](https://doi.org/10.5281/zenodo.1069648)
- Crnojević, D., Sand, D. J., Caldwell, N., et al. 2014, *ApJL*, 795, L35, doi: [10.1088/2041-8205/795/2/L35](https://doi.org/10.1088/2041-8205/795/2/L35)
- Crnojević, D., Sand, D. J., Spekkens, K., et al. 2016, *ApJ*, 823, 19, doi: [10.3847/0004-637X/823/1/19](https://doi.org/10.3847/0004-637X/823/1/19)
- Crnojević, D., Sand, D. J., Bennet, P., et al. 2019, *ApJ*, 872, 80, doi: [10.3847/1538-4357/aafbe7](https://doi.org/10.3847/1538-4357/aafbe7)
- Da Costa, G. S., & Armandroff, T. E. 1990, *AJ*, 100, 162, doi: [10.1086/115500](https://doi.org/10.1086/115500)
- Dey, A., Schlegel, D. J., Lang, D., et al. 2019, *AJ*, 157, 168, doi: [10.3847/1538-3881/ab089d](https://doi.org/10.3847/1538-3881/ab089d)
- Dressler, A., Hare, T., Bigelow, B. C., & Osip, D. J. 2006, in *Society of Photo-Optical Instrumentation Engineers (SPIE) Conference Series*, Vol. 6269, *Society of Photo-Optical Instrumentation Engineers (SPIE) Conference Series*, ed. I. S. McLean & M. Iye, 62690F, doi: [10.1117/12.670573](https://doi.org/10.1117/12.670573)
- Drlica-Wagner, A., Bechtol, K., Rykoff, E. S., et al. 2015, *ApJ*, 813, 109, doi: [10.1088/0004-637X/813/2/109](https://doi.org/10.1088/0004-637X/813/2/109)
- Drlica-Wagner, A., Carlin, J. L., Nidever, D. L., et al. 2021, *ApJS*, 256, 2, doi: [10.3847/1538-4365/ac079d](https://doi.org/10.3847/1538-4365/ac079d)
- Du, W., & McGaugh, S. S. 2020, *AJ*, 160, 122, doi: [10.3847/1538-3881/aba754](https://doi.org/10.3847/1538-3881/aba754)
- Dutton, A. A., Macciò, A. V., Frings, J., et al. 2016, *MNRAS*, 457, L74, doi: [10.1093/mnrasl/slv193](https://doi.org/10.1093/mnrasl/slv193)
- Fitts, A., Boylan-Kolchin, M., Elbert, O. D., et al. 2017, *MNRAS*, 471, 3547, doi: [10.1093/mnras/stx1757](https://doi.org/10.1093/mnras/stx1757)
- Gaia Collaboration, Prusti, T., de Bruijne, J. H. J., et al. 2016, *A&A*, 595, A1, doi: [10.1051/0004-6361/201629272](https://doi.org/10.1051/0004-6361/201629272)
- Gaia Collaboration, Vallenari, A., Brown, A. G. A., et al. 2023, *A&A*, 674, A1, doi: [10.1051/0004-6361/202243940](https://doi.org/10.1051/0004-6361/202243940)
- Garrison-Kimmel, S., Wetzel, A., Bullock, J. S., et al. 2017, *MNRAS*, 471, 1709, doi: [10.1093/mnras/stx1710](https://doi.org/10.1093/mnras/stx1710)
- Ginsburg, A., Sipőcz, B. M., Brasseur, C. E., et al. 2019, *AJ*, 157, 98, doi: [10.3847/1538-3881/aafc33](https://doi.org/10.3847/1538-3881/aafc33)
- Giovanelli, R., & Haynes, M. P. 2015, *A&A Rv*, 24, 1, doi: [10.1007/s00159-015-0085-3](https://doi.org/10.1007/s00159-015-0085-3)
- Giovanelli, R., Haynes, M. P., Kent, B. R., et al. 2005, *AJ*, 130, 2598, doi: [10.1086/497431](https://doi.org/10.1086/497431)
- Giovanelli, R., Haynes, M. P., Adams, E. A. K., et al. 2013, *AJ*, 146, 15, doi: [10.1088/0004-6256/146/1/15](https://doi.org/10.1088/0004-6256/146/1/15)
- Haynes, M. P., Giovanelli, R., Kent, B. R., et al. 2018, *ApJ*, 861, 49, doi: [10.3847/1538-4357/aac956](https://doi.org/10.3847/1538-4357/aac956)
- Hoversten, E. A., Gronwall, C., Vanden Berk, D. E., et al. 2009, *ApJ*, 705, 1462, doi: [10.1088/0004-637X/705/2/1462](https://doi.org/10.1088/0004-637X/705/2/1462)
- Hunter, J. D. 2007, *Computing in Science and Engineering*, 9, 90, doi: [10.1109/MCSE.2007.55](https://doi.org/10.1109/MCSE.2007.55)
- Iglesias-Páramo, J., Buat, V., Takeuchi, T. T., et al. 2006, *ApJS*, 164, 38, doi: [10.1086/502628](https://doi.org/10.1086/502628)
- Irwin, M. J., Belokurov, V., Evans, N. W., et al. 2007, *ApJL*, 656, L13, doi: [10.1086/512183](https://doi.org/10.1086/512183)
- Jeřábková, T., Hasani Zonoozi, A., Kroupa, P., et al. 2018, *A&A*, 620, A39, doi: [10.1051/0004-6361/201833055](https://doi.org/10.1051/0004-6361/201833055)
- Joye, W. A., & Mandel, E. 2003, in *Astronomical Society of the Pacific Conference Series*, Vol. 295, *Astronomical Data Analysis Software and Systems XII*, ed. H. E. Payne, R. I. Jedrzejewski, & R. N. Hook, 489
- Kalberla, P. M. W., & Haud, U. 2015, *A&A*, 578, A78, doi: [10.1051/0004-6361/201525859](https://doi.org/10.1051/0004-6361/201525859)
- Karachentsev, I. D., & Kaisina, E. I. 2019, *Astrophysical Bulletin*, 74, 111, doi: [10.1134/S1990341319020019](https://doi.org/10.1134/S1990341319020019)
- Klypin, A., Kravtsov, A. V., Valenzuela, O., & Prada, F. 1999, *ApJ*, 522, 82, doi: [10.1086/307643](https://doi.org/10.1086/307643)
- Koposov, S. E., Belokurov, V., Torrealba, G., & Evans, N. W. 2015, *ApJ*, 805, 130, doi: [10.1088/0004-637X/805/2/130](https://doi.org/10.1088/0004-637X/805/2/130)
- Koribalski, B. S., Staveley-Smith, L., Westmeier, T., et al. 2020, *Ap&SS*, 365, 118, doi: [10.1007/s10509-020-03831-4](https://doi.org/10.1007/s10509-020-03831-4)
- Lang, D., Hogg, D. W., Mierle, K., Blanton, M., & Roweis, S. 2010, *AJ*, 139, 1782, doi: [10.1088/0004-6256/139/5/1782](https://doi.org/10.1088/0004-6256/139/5/1782)

- Lee, M. G., Freedman, W. L., & Madore, B. F. 1993, *ApJ*, 417, 553, doi: [10.1086/173334](https://doi.org/10.1086/173334)
- Makarov, D., Makarova, L., Rizzi, L., et al. 2006, *AJ*, 132, 2729, doi: [10.1086/508925](https://doi.org/10.1086/508925)
- Martin, N. F., de Jong, J. T. A., & Rix, H.-W. 2008, *ApJ*, 684, 1075, doi: [10.1086/590336](https://doi.org/10.1086/590336)
- Martínez-Delgado, D., Karim, N., Charles, E. J. E., et al. 2022, *MNRAS*, 509, 16, doi: [10.1093/mnras/stab2797](https://doi.org/10.1093/mnras/stab2797)
- McClure-Griffiths, N. M., Pisano, D. J., Calabretta, M. R., et al. 2009, *ApJS*, 181, 398, doi: [10.1088/0067-0049/181/2/398](https://doi.org/10.1088/0067-0049/181/2/398)
- McConnachie, A. W., Huxor, A., Martin, N. F., et al. 2008, *ApJ*, 688, 1009, doi: [10.1086/591313](https://doi.org/10.1086/591313)
- McGaugh, S. S. 2012, *AJ*, 143, 40, doi: [10.1088/0004-6256/143/2/40](https://doi.org/10.1088/0004-6256/143/2/40)
- McNanna, M., Bechtol, K., Mau, S., et al. 2023, arXiv e-prints, arXiv:2309.04467, doi: [10.48550/arXiv.2309.04467](https://doi.org/10.48550/arXiv.2309.04467)
- McQuinn, K. B. W., Mao, Y.-Y., Cohen, R. E., et al. 2023, arXiv e-prints, arXiv:2307.08738, doi: [10.48550/arXiv.2307.08738](https://doi.org/10.48550/arXiv.2307.08738)
- McQuinn, K. B. W., Cannon, J. M., Dolphin, A. E., et al. 2014, *ApJ*, 785, 3, doi: [10.1088/0004-637X/785/1/3](https://doi.org/10.1088/0004-637X/785/1/3)
- McQuinn, K. B. W., Skillman, E. D., Dolphin, A., et al. 2015a, *ApJ*, 812, 158, doi: [10.1088/0004-637X/812/2/158](https://doi.org/10.1088/0004-637X/812/2/158)
- McQuinn, K. B. W., Cannon, J. M., Dolphin, A. E., et al. 2015b, *ApJ*, 802, 66, doi: [10.1088/0004-637X/802/1/66](https://doi.org/10.1088/0004-637X/802/1/66)
- Millman, K. J., & Aivazis, M. 2011, *Computing in Science and Engineering*, 13, 9, doi: [10.1109/MCSE.2011.36](https://doi.org/10.1109/MCSE.2011.36)
- Moore, B. 1994, *Nature*, 370, 629, doi: [10.1038/370629a0](https://doi.org/10.1038/370629a0)
- Müller, O., Rejkuba, M., Pawłowski, M. S., et al. 2019, *A&A*, 629, A18, doi: [10.1051/0004-6361/201935807](https://doi.org/10.1051/0004-6361/201935807)
- Mutlu-Pakdil, B., Sand, D. J., Carlin, J. L., et al. 2018, *ApJ*, 863, 25, doi: [10.3847/1538-4357/aacd0e](https://doi.org/10.3847/1538-4357/aacd0e)
- Mutlu-Pakdil, B., Sand, D. J., Crnojević, D., et al. 2021, *ApJ*, 918, 88, doi: [10.3847/1538-4357/ac0db8](https://doi.org/10.3847/1538-4357/ac0db8)
- . 2022, *ApJ*, 926, 77, doi: [10.3847/1538-4357/ac4418](https://doi.org/10.3847/1538-4357/ac4418)
- Oliphant, T. E. 2007, *Computing in Science and Engineering*, 9, 10, doi: [10.1109/MCSE.2007.58](https://doi.org/10.1109/MCSE.2007.58)
- pandas development team, T. 2020, *pandas-dev/pandas: Pandas, latest*, Zenodo, doi: [10.5281/zenodo.3509134](https://doi.org/10.5281/zenodo.3509134)
- Pawłowski, M. S., Pflamm-Altenburg, J., & Kroupa, P. 2012, *MNRAS*, 423, 1109, doi: [10.1111/j.1365-2966.2012.20937.x](https://doi.org/10.1111/j.1365-2966.2012.20937.x)
- Peng, C. Y., Ho, L. C., Impey, C. D., & Rix, H.-W. 2002, *AJ*, 124, 266, doi: [10.1086/340952](https://doi.org/10.1086/340952)
- . 2010, *AJ*, 139, 2097, doi: [10.1088/0004-6256/139/6/2097](https://doi.org/10.1088/0004-6256/139/6/2097)
- Pflamm-Altenburg, J., & Kroupa, P. 2009, *ApJ*, 706, 516, doi: [10.1088/0004-637X/706/1/516](https://doi.org/10.1088/0004-637X/706/1/516)
- Rey, M. P., Pontzen, A., Agertz, O., et al. 2020, *MNRAS*, 497, 1508, doi: [10.1093/mnras/staa1640](https://doi.org/10.1093/mnras/staa1640)
- . 2022, *MNRAS*, 511, 5672, doi: [10.1093/mnras/stac502](https://doi.org/10.1093/mnras/stac502)
- Rhode, K. L., Salzer, J. J., Haurberg, N. C., et al. 2013, *AJ*, 145, 149, doi: [10.1088/0004-6256/145/6/149](https://doi.org/10.1088/0004-6256/145/6/149)
- Robitaille, T., Deil, C., & Ginsburg, A. 2020, reproject: Python-based astronomical image reprojection. <http://ascl.net/2011.023>
- Sales, L. V., Wetzell, A., & Fattahi, A. 2022, *Nature Astronomy*, 6, 897, doi: [10.1038/s41550-022-01689-w](https://doi.org/10.1038/s41550-022-01689-w)
- Sánchez, E., & Des Collaboration. 2010, in *Journal of Physics Conference Series*, Vol. 259, *Journal of Physics Conference Series*, 012080, doi: [10.1088/1742-6596/259/1/012080](https://doi.org/10.1088/1742-6596/259/1/012080)
- Sand, D. J., Spekkens, K., Crnojević, D., et al. 2015, *ApJL*, 812, L13, doi: [10.1088/2041-8205/812/1/L13](https://doi.org/10.1088/2041-8205/812/1/L13)
- Sand, D. J., Strader, J., Willman, B., et al. 2012, *ApJ*, 756, 79, doi: [10.1088/0004-637X/756/1/79](https://doi.org/10.1088/0004-637X/756/1/79)
- Sand, D. J., Crnojević, D., Strader, J., et al. 2014, *ApJL*, 793, L7, doi: [10.1088/2041-8205/793/1/L7](https://doi.org/10.1088/2041-8205/793/1/L7)
- Sand, D. J., Mutlu-Pakdil, B., Jones, M. G., et al. 2022, *ApJL*, 935, L17, doi: [10.3847/2041-8213/ac85ee](https://doi.org/10.3847/2041-8213/ac85ee)
- Sawala, T., Frenk, C. S., Fattahi, A., et al. 2016, *MNRAS*, 457, 1931, doi: [10.1093/mnras/stw145](https://doi.org/10.1093/mnras/stw145)
- Schlaflly, E. F., & Finkbeiner, D. P. 2011, *ApJ*, 737, 103, doi: [10.1088/0004-637X/737/2/103](https://doi.org/10.1088/0004-637X/737/2/103)
- Schlegel, D. J., Finkbeiner, D. P., & Davis, M. 1998, *ApJ*, 500, 525, doi: [10.1086/305772](https://doi.org/10.1086/305772)
- Simon, J. D. 2019, *ARA&A*, 57, 375, doi: [10.1146/annurev-astro-091918-104453](https://doi.org/10.1146/annurev-astro-091918-104453)
- Simpson, C. M., Bryan, G. L., Johnston, K. V., et al. 2013, *MNRAS*, 432, 1989, doi: [10.1093/mnras/stt474](https://doi.org/10.1093/mnras/stt474)
- Smercina, A., Bell, E. F., Price, P. A., et al. 2018, *ApJ*, 863, 152, doi: [10.3847/1538-4357/aad2d6](https://doi.org/10.3847/1538-4357/aad2d6)
- Smercina, A., Bell, E. F., Slater, C. T., et al. 2017, *ApJL*, 843, L6, doi: [10.3847/2041-8213/aa78fa](https://doi.org/10.3847/2041-8213/aa78fa)
- Stetson, P. B. 1987, *PASP*, 99, 191, doi: [10.1086/131977](https://doi.org/10.1086/131977)
- . 1994, *PASP*, 106, 250, doi: [10.1086/133378](https://doi.org/10.1086/133378)
- Taylor, E. N., Hopkins, A. M., Baldry, I. K., et al. 2011, *MNRAS*, 418, 1587, doi: [10.1111/j.1365-2966.2011.19536.x](https://doi.org/10.1111/j.1365-2966.2011.19536.x)
- Tollerud, E. J., & Peek, J. E. G. 2018, *ApJ*, 857, 45, doi: [10.3847/1538-4357/aab3e4](https://doi.org/10.3847/1538-4357/aab3e4)
- van der Walt, S., Colbert, S. C., & Varoquaux, G. 2011, *Computing in Science and Engineering*, 13, 22, doi: [10.1109/MCSE.2011.37](https://doi.org/10.1109/MCSE.2011.37)
- Wes McKinney. 2010, in *Proceedings of the 9th Python in Science Conference*, ed. Stéfan van der Walt & Jarrod Millman, 56 – 61, doi: [10.25080/Majora-92bf1922-00a](https://doi.org/10.25080/Majora-92bf1922-00a)

- Wetzell, A. R., Hopkins, P. F., Kim, J.-h., et al. 2016, ApJL, 827, L23, doi: [10.3847/2041-8205/827/2/L23](https://doi.org/10.3847/2041-8205/827/2/L23)
- Wheeler, C., Oñorbe, J., Bullock, J. S., et al. 2015, MNRAS, 453, 1305, doi: [10.1093/mnras/stv1691](https://doi.org/10.1093/mnras/stv1691)
- Willman, B., Dalcanton, J. J., Martinez-Delgado, D., et al. 2005, ApJL, 626, L85, doi: [10.1086/431760](https://doi.org/10.1086/431760)
- York, D. G., Adelman, J., Anderson, John E., J., et al. 2000, AJ, 120, 1579, doi: [10.1086/301513](https://doi.org/10.1086/301513)
- Zaritsky, D., Donnerstein, R., Dey, A., et al. 2023, ApJS, 267, 27, doi: [10.3847/1538-4365/acdd71](https://doi.org/10.3847/1538-4365/acdd71)
- Zaritsky, D., Donnerstein, R., Karunakaran, A., et al. 2021, ApJS, 257, 60, doi: [10.3847/1538-4365/ac2607](https://doi.org/10.3847/1538-4365/ac2607)
- . 2022, ApJS, 261, 11, doi: [10.3847/1538-4365/ac6ceb](https://doi.org/10.3847/1538-4365/ac6ceb)
- Zaritsky, D., Donnerstein, R., Dey, A., et al. 2019, ApJS, 240, 1, doi: [10.3847/1538-4365/aaefe9](https://doi.org/10.3847/1538-4365/aaefe9)
- Zhang, K., Wu, J., Li, D., et al. 2021, MNRAS, 500, 1741, doi: [10.1093/mnras/staa3275](https://doi.org/10.1093/mnras/staa3275)
- Zibetti, S., Charlot, S., & Rix, H.-W. 2009, MNRAS, 400, 1181, doi: [10.1111/j.1365-2966.2009.15528.x](https://doi.org/10.1111/j.1365-2966.2009.15528.x)